Hybrid Heterojunction Nanorods for Nanoscale Controlled Morphology in Bulk Heterojunction Solar Cells

ARTICLE *in* THE JOURNAL OF PHYSICAL CHEMISTRY C · MAY 2011

Impact Factor: 4.77 · DOI: 10.1021/jp112369t

16 AUTHORS, INCLUDING:

Mingqing Wang
Dalhousie University
18 PUBLICATIONS **261** CITATIONS
SEE PROFILE

Cyril Martini
Collège de France
18 PUBLICATIONS **191** CITATIONS
SEE PROFILE

Hugues Brisset
Université de Toulon
91 PUBLICATIONS **1,242** CITATIONS
SEE PROFILE

Jörg Ackermann
Aix-Marseille Université
75 PUBLICATIONS **861** CITATIONS
SEE PROFILE

THE JOURNAL OF PHYSICAL CHEMISTRY C

ARTICLE

pubs.acs.org/JPCC

Hybrid Heterojunction Nanorods for Nanoscale Controlled Morphology in Bulk Heterojunction Solar Cells

Jose Mawyin,[†] Ivan Shupyk,[†] Mingqing Wang,[†] Guillaume Poize,[†] Pedro Atienzar,[‡] Thilini Ishwara,[‡] James R. Durrant,[‡] Jenny Nelson,[‡] Daiki Kanehira,[§] Noriyuki Yoshimoto,[§] Cyril Martini,[†] Ekaterina Shilova,[†] Patrick Secondo,[†] Hugues Brisset,[†] Frederic Fages,*[,†] and Jörg Ackermann*[,†]

[†]Centre Interdisciplinaire de Nanoscience de Marseille, CINaM, UPR CNRS 3118, Université de la Méditerranée, Campus de Luminy, Case 913. France

[‡]Centre for Electronic Materials and Devices, Imperial College London, London SW7 2AZ, United Kingdom

[§]Department of Materials Science and Engineering, Iwate University, Ueda Morioka 020-8551, Japan

Supporting Information

ABSTRACT: In this study, we report bulk heterojunction solar cells using hybrid heterojunction nanorods as photoactive material. The core−shell nanorods are obtained via self-assembly of low band gap p-type oligomers onto ZnO nanorod surfaces. This produces highly soluble donor−acceptor nanostructures that feature a grafted p-type semiconducting monolayer with a band gap of 2.1 eV. The solution processing of the coaxial nanorods into thin films leads to bulk heterojunctions of particularly large donor−acceptor interfaces. Importantly by simple processing donor domains smaller than typical exciton diffusion length of organic semiconductors are obtained which guaranties efficient exciton dissociation. The corresponding solar cells reveal that the hydrid nanorod layers form efficient interpenetrated networks which lead to external quantum efficiency of 20% at the absorption maximum λ_{max} = 498 nm. Although the donor domains of these hybrid bulk heterojunction are constituted by monolayers, transient absorption spectroscopy could evidence long-lived photoinduced charge carrier generation of significant intensity. Thus the described hybrid heterojunction nanorods represent a promising strategy toward nanoscale controlled bulk heterojunction solar cells.

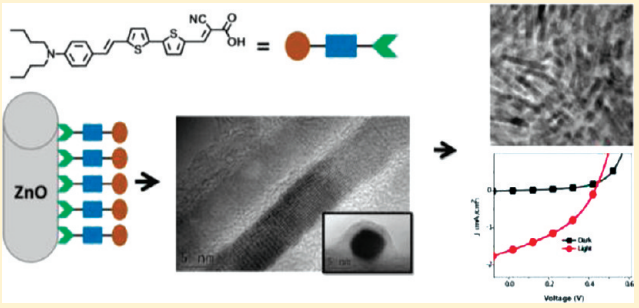

1. INTRODUCTION

The introduction of nanoscale architecture by mixing organic electron donor and acceptor materials in what is called the bulk heterojunction (BHJ)[1−3] is currently one of the most promising approaches to fabricate efficient low-cost organic solar cells. Intensive studies during the past decade have continuously increased the efficiency of organic BHJ devices,[4] and world record cells show today 8.13% solar energy conversion efficiency[5] indicating clearly their potential for future applications. An interesting alternative to these all-organic solar cells is the hybrid BHJ approach, which replaces the organic acceptor material by inorganic n-type nanoparticles. Such hybrid solar cells aim to combine the versatile solution processing of conjugated polymers with the high electron mobility and good physical and chemical stability of inorganic semiconductors.[6] The photoactive layer of a hybrid BHJ solar cell is usually obtained by blending donor polymers and n-type inorganic nanoparticles that phase separate during film deposition into a network of n-type nanoparticles surrounded by the polymer matrix. Different inorganic semiconductors such as CdSe,[7,8] TiO_2,[9−16] ZnO,[17−22] PbS,[23,24] and silicon[25,26] nanoparticles have been combined with p-type polymers and efficiencies of 3.2% were demonstrated recently.

The performance of hybrid BHJ solar cells depends strongly on the nanoscale morphology of the active layer. Intensive studies have been devoted to methods for improving the morphology of hybrid polymer blends.[20,26−32] Among them, surface capping ligands play a important role by tailoring the compatibility of the nanoparticles with the polymer host, which finally controls the morphologies of the two phases and, thus, the efficiency of charge creation and transport.[27,33] However, such capping ligands also influence the connectivity between nanoparticles, which can lead to poor device performance, although the dispersion of the nanoparticles inside the polymer is improved.[17] Moreover, capping surfactants form interfacial layers between the nanoparticle and the polymer, which influence many relevant parameters of the hybrid interface such as exciton dissociation, charge carrier injection, and recombination kinetics. For example, interfacial nanostructuring of TiO_2 nanorods by

Received: December 29, 2010
Revised: April 7, 2011
Published: May 06, 2011

grafting electroactive surfactants in polyl(3-hexylthiophene) (P3HT)/TiO_2 blends increases device performance by reducing recombination kinetics.[15] Recently, we have demonstrated that dye surfactants in (P3HT)/ZnO blends are able to contribute directly to the photocurrent generation and increase the spectral response of the solar cells. Unfortunately, we found that the dye grafting increases aggregation between nanoparticles at the same time leading finally to strong losses in the device performance.[20] It is obvious that in polymer blends capping surfactants control the polymer−nanoparticle and the nanoparticle−nanoparticle interface as well as the nanoscale morphology of blend simultaneously, which makes it difficult to optimize hybrid polymer blend solar cells by this unique tool.

This work presents hybrid solar cells, which use inorganic n-type nanoparticles bearing p-type oligomer surfactants directly as active materials, thus eliminating the need of blending the nanoparticles with a p-type polymer. These solar cells allow simple processing of BHJ layers independent of the solvent or the deposition conditions with donor phases below typical exciton diffusion lengths, while the hybrid interface between the nanoparticles and the grafted donor is controlled at a molecular scale. Recently, we have shown that self-assembly of p-type biothiophene derivative monolayers[34] onto ZnO nanorods leads to coaxial p−n junction core−shell systems.[35] These coaxial structures representing nanometer scale sized bulk heterojunctions could be solution-processed into thin films with ambipolar charge transport properties, i.e., holes and electrons are transported by the grafted molecules and the ZnO nanorods, respectively. At that time, however, the light absorption properties of the coaxial nanostructures were not yet adapted for PV applications. A first application of hybrid coaxial nanostructures in photovoltaics has been given very recently by Yang et al. who demonstrated single coaxial nanowire solar cells based on ZnO nanowires modified with polythiophene derivatives.[36] Here, we report the synthesis of low band gap bithiophene derivative surfactant with suitable absorption properties in the visible and corresponding hybrid p−n junction core−shell nanosystems from which we subsequently fabricated solution processed BHJ solar cells with donor domains in monolayer dimensions and efficient photocurrent generation. A complete set of experiments is presented to elucidate the morphological and photovoltaic properties of this new approach to form BHJ solar cells.

EXPERIMENTAL SECTION

Synthesis of the Low Band Gap Oligomer 1. The synthesis of molecule **1** is detailed in the Supporting Information.

Synthesis of ZnO Nanorods. ZnO nanorods were prepared according to a published procedure.[36] Zinc acetate (99.99%) and sodium hydroxyde (99.998%)) were purchased from Aldrich. Methanol was distilled on CaO. All the glassware was washed with a concentrated solution of sodium hydroxide and rinsed with deionized water prior to use. In a typical experiment, sodium hydroxide (289 mg, 7.22 mmol) and methanol (23 mL) were sonicated until a fine dispersion was obtained. Separately, zinc acetate (818 mg, 4.46 mmol), methanol (42 mL), and water (318 mL) were introduced in a glass flask, sonicated until complete dissolution, and heated under stirring to 60 °C under argon atmosphere. The sodium hydroxide solution was then added dropwise. After 2 h and 15 min at 60 °C, the growth solution was condensed to 10 mL under reduced pressure at 55 °C (until the solution became colorless). This condensation step creates the seed solution from which NRs are grown. The reaction mixture was heated for 48 h at 60 °C to grow the nanorods. Then, the nanorods were separated from the seed solution by several precipitation and washing steps using methanol. Finally the ZnO nanorods were transferred to chloroforme by centrifugation.

Solar Cell Fabrication and Characterization. Solar cells were prepared with the temperature and atmosphere at room conditions. The devices were prepared on top of ITO glass substrate that has a sheet resistivity of 30 Ω/square. A thin layer (∼100 nm) of PEDOT−PSS (poly(ethylenedioxythiophene)−poly(styrenesulfonate)) (H-Starck, Germany) was spin coated (5000 rpm for 50 s) on top of the ITO to serve as a hole-only transport layer while also aiding to smooth out the ITO surface. The PEDOT−PSS layer was subsequently annealed in air at 140 °C during 10 min. Then **1** and ZnO NR are mixed in chlorobenzene with **1** weight percentage from 14 to 28% in **1:ZnO** using a ZnO concentration of 30 mg/mL. The photoactive solution was continuously sonicated in a water bath at 50 °C before spin coating. The **1**−**ZnO** solution was spin coated (1500 rpm for 20 s) on top of the PEDOT−PSS layer and allowed to dry under argon. The final step is the deposition of electrodes through evaporation of aluminum (80 nm) under vacuum. $I-V$ measurements were performed in the dark and under 100 mW/cm^2 of AM1.5 illumination using a 150 W class AAA simulator from Oriel. External quantum efficiency measurements (EQE) were measured in air using a white-light halogen tungsten source combined with a Cornerstone monochromator with the spectral intensity calibrated using a reference silicon solar cell. For the calculation of the internal quantum efficiency, the total absorption of the solar cell was obtained by measuring reflection of the device with a Varian Cary 5000 combined with an external integral sphere. The device absorption corresponds to the double pathway in the **1**−**ZnO** and PEDOT−PSS layer as a result of reflection from the aluminum electrode.

Optical Characterization in Solution and Thin Films. UV−vis absorption and fluorescence investigations of the nanohybrids in solution and thin films were recorded using a Varian CARY 50 spectrophotometer and a CARY Eclipse spectrometer, respectively.

High-Resolution Transmission Electron Microscope (HR-TEM). A HR-TEM JEOL 3010 (operating at an acceleration voltage of 300 kV) was used to study the morphology of **1**−**ZnO** nanorods and the corresponding thin films. Samples of **1**−**ZnO** nanorods were prepared by drop casting a diluted solution of grafted nanorods on carbon-coated TEM grids. The organic **1** layer could be clearly seen when the ZnO nanorods where positioned perpendicular to the plane of the observation (axial view). In the case of HR-TEM analysis of spin coated thin films, the photoactive layer was first spin coated onto a PEDOT−PSS layer, followed by placing the layer on top of carbon-coated TEM grids after dissolving the PEDOT−PSS layer in deionized water.

X-ray Diffraction Analysis (XRD). XRD analysis are performed in in-plane (IP-XRD) and out-of-plane (OOP-XRD) configuration using an X-ray diffractometer (Regaku Co., ATX-G), equipped with a multilayered X-ray mirror used to radiate a collimated parallel beam. The goniometer has not only conventional $\theta/2\theta$ axes but also in-plane $\theta/2\theta\chi$ axes. The wavelength of X-ray beam used for measurement was 0.1542 nm. All PV characterizations were performed under an inert argon atmosphere.

Transient Absorption Spectroscopy (TAS). The charge transfer properties of the blend films were investigated through

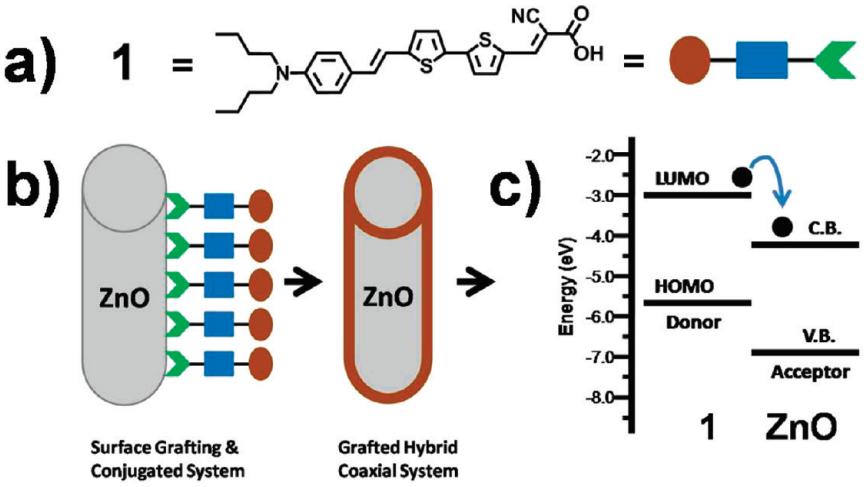

Figure 1. (a) Molecular structure of compound **1**. (b) Grafting of compound **1** to the surface of ZnO nanorods forming a coaxial heterojunction. (c) Energy diagram of the coaxial heterojunction **1**−**ZnO**.

microsecond−millisecond TAS using an experimental configuration described elsewhere.[8] For this system, the excitation (nitrogen-pumped dye laser, repetition rate ∼4 Hz, pulse duration <1 ns) was set to 520 nm, with a pump energy density of 45 $mJ \cdot cm^{-2} \cdot pulse^{-1}$. The transient absorption spectra were monitored by changing the probe wavelength (tungsten lamp) between 680 and 950 nm.

Cyclic Voltammetry (CV). CV was recording with a BAS 100 potentiostat (Bioanalytical Systems) operated with BAS 100W (v2.3) software. A three-electron setup based on a Pt working electrode (diameter 0.1 mm), a Pt counter electrode, and a Ag/AgCl (filled with 3 M NaCl) was used. Tetrabutylammonium hexafluorophosphate (TBAPF6) (Fluka) was used as received as electrolyte (0.1 M). All experiments were carried out in 1, 2-dichlorobenzene at 50 °C. $E_{1/2}$ redox values are determined from the cyclic voltammogram at a scan rate of 50 $mV \cdot s^{-1}$. Ferrocene was used as internal standard.

RESULTS AND DISCUSSION

To obtain hybrid coaxial nanorods with suitable photovoltaic and processing properties, the choice of the p-type surfactant is important. The molecule has to fulfill three tasks: first to strongly absorb light in the visible spectrum, second form a hybrid heterojunction interface with suitable energy alignment for exciton dissociation, and third transport hole efficiently after successful exciton dissociation. Additionally, the molecule has to promote high solubility to the nanorods once grafted, which is important for solution processing of the coaxial nanorods into thin films. Previously, we reported coaxial nanohybrids with crystalline organization and strong $\pi-\pi$ stacking among grafted molecules at the ZnO nanorod surface. The crystalline organization was promoted by the presence of an *n*-octyloxy chain at the terminal phenyl para position in a bithiophene derivative.[35] This led to densely packed H-aggregates causing strong hypsochromic shift in the absorption spectrum of the compound that was unfavorable for PV applications. Such strong hypsochromic shifts upon H-aggregation are well-known for oligothiophene derivative. To improve the optical properties of the SAM, strong H-aggregation among grafted molecules has to be avoided and a more amorphous organization within the SAM obtained. Indeed, amorphous

Figure 2. Optical image of chloroform solutions containing ZnO nanorods (right) and **1**−**ZnO** nanorods (left). The concentration of ZnO in both cases is 10 mg/mL chloroform.

organic semiconductors with high charge carrier mobilities and conversion efficiencies in organic bilayer and bulk heterojunction solar cells up to 2.2% could be demonstrated recently,[37−39] indicating that highly crystalline organization is not necessary for efficient solar cells. Therefore, we used the *N*,*N*-di-*n*-butylamino end group in order to introduce some steric effects between neighboring oligomers and, in turn, to avoid crystalline aggregation (Figure 1a). This substituent also promotes high solubility of the coaxial nanorods once grafted. Moreover it plays the role of the electron donor group in the push−pull structure, which is needed to reduce the band gap of the SAM as shown in Figure 1a. The carboxylic acid group directly substituted to the π-conjugated system is chosen as grafting unit to obtain efficient electron injection into metal oxide nanostructures. Cyclic voltammetry was used to determine the energy level of the molecule. The CV of **1** given in Figure S1 (Supporting Information) shows four one-electron process waves corresponding to the formation of cation, cation radical, anion, and anion radical at $E_{1/2}(ox1)$ = 0.06 V, $E_{1/2}(ox2)$ = 0.41 V, $E_{1/2}(red1)$ = −2,15 V, and $E_{1/2}(red2)$ = −2,41 vs ferrocene/ferricinium (Fc/Fc^{+}), respectively. By using equation $E_{HOMO} = -4.84 - E_{1/2}(ox1)$ and $E_{LUMO} = -4.84 + E_{1/2}(red1)$,[40] the highest occupied molecular orbital (HOMO) and the lowest unoccupied molecular orbital (LUMO) levels of **1** were found to be 4.9 and 2.7 eV, respectively. These values are close to values obtained for other p-type

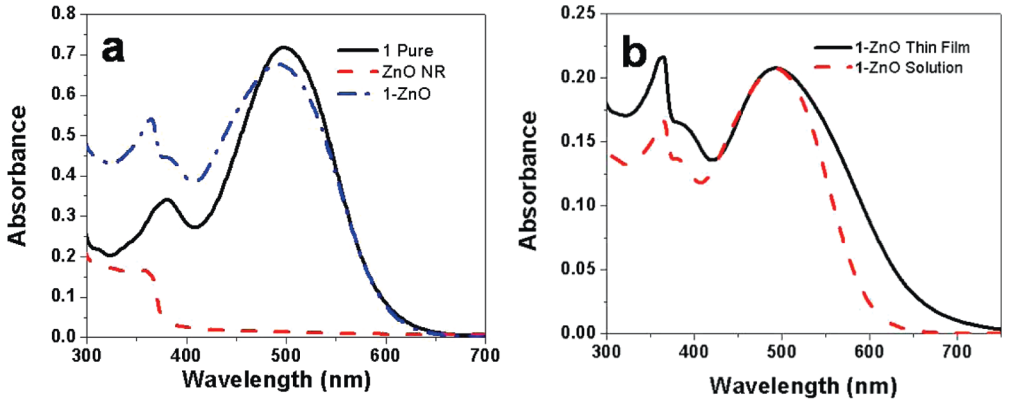

Figure 3. (a) Absorption spectra of ZnO nanorods, compound **1** and **1**−**ZnO** nanohybrids in chlorobenzene solution. (b) Absorption spectra of **1**−**ZnO** in solution and corresponding **1**−**ZnO** thin film, which was obtained by spin coating **1**−**ZnO** chlorobenzene solution onto glass substrates. The spectrum of **1**−**ZnO** in solution was normalized at the absorption maximum of **1**−**ZnO** films for comparison.

semiconductors of such a family of molecules using cyano groups or carboxylic acid groups indicating the electron donating character of **1**.[41,26] To form a coaxial heterojunction, we used ZnO nanorods as the electron acceptor and scaffold for SAM formation due to their straightforward synthesis and advantageous properties such as air stability, high electron mobility, and environmental. Additionally, nanorods introduce transport channels of charges along their *c* axis, which is expected to improve PV properties compared to spherical nanoparticles. The ZnO nanorods are synthesized using a hydrothermal technique as reported recently exhibiting average length of 40 nm and diameter of 6 nm leading to an aspect ratio ∼7:1.[35]

Figure 1c shows the energy diagram of the coaxial nanorods **1**−**ZnO** taking into account the energy level of molecule **1** and ZnO.[42] The large band offset between the LUMO level of molecule **1** and the conduction band of the ZnO represents a strong driving force for exciton at the hybrid interface.[41]

Coaxial Nanorod Synthesis and Analysis. The coaxial **1**−**ZnO** heterojunctions are produced by simply mixing ZnO nanorods and compound **1** in chlorobenzene (Figure 1b). Grafting of **1** onto the ZnO nanoords is first visualized by optical changes of the solution. Prior to grafting, ZnO nanorods form aggregates in solution as indicated by strong light scattering of the solution (Figure 2). Once **1** is grafted, the solubility of the hybrid nanorods increased dramatically so that stable solutions of **1**−**ZnO** with concentrations up to 60 mg/mL can be obtained in chlorobenzene (Figure 2). The formation of **1**−**ZnO** was further investigated by absorption spectroscopy. Figure 3a compares the absorption spectra of molecule **1**, ZnO nanorods, and **1**−**ZnO** in chlorobenzene solution. The absorption maximum of compound **1** is located at λ_{max} = 498 nm. The measured spectrum of **1**−**ZnO** corresponds principally to the combined molecule and ZnO absorption peaks. However the grafted molecules show a broader absorption band with a hypsochromic shift of 5 nm compared to **1** in solution. This weak shift is in contrast to our early work where highly a pronounced hypsochromic shift in the absorption of the grafted molecule was observed.[35] The optical band gap of **1**−**ZnO** was calculated to 2.1 eV using the onset of the grafted molecule absorption band. High-resolution transmission electron microscopy (HR-TEM) analysis was used to visualize the coaxial morphology of the nanostructure. Panels a and b of Figure 4 show HR-TEM analysis of the hybrid nanorods lying flat on the carbon grid or in up-standing position so that a view along

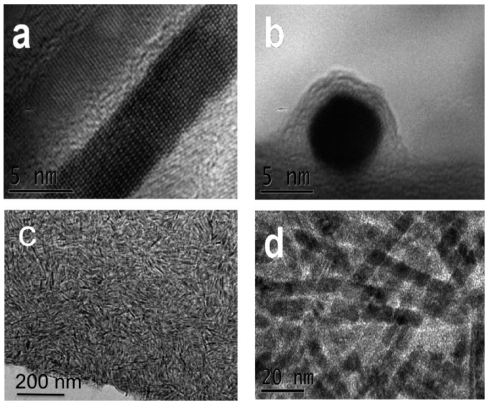

Figure 4. High-resolution transmission electron microscope images of **1**−**ZnO** nanorods showing (a) crystalline planes of ZnO nanorods and the small gap between rods produced by the organic shell; (b) view along the *c* axis of a nanorod showing ZnO core and organic shell. (c, d) Top views of **1**−**ZnO** active layer. The layers were first spin coated onto PEDOT−PSS covered ITO substrates, then removed by dissolving PEDOT−PSS in water and finally transferred onto a carbon grid.

the rode axis is visible. Both figures show the formation of a **1** monolayer around the ZnO nanorod. The total diameter of the **1**−**ZnO** is determined to 10 nm, which corresponds to an average ZnO nanorod diameter of 6 nm as well as twice thickness of the grafted monolayer of 2 nm. Interestingly if one looks more in detail on the morphology of the SAM in Figure 4b, one can see that the SAM shows a constant thickness around the rod only in the areas, which are not in contact with the carbon grid. Directly at the contact between the SAM and the carbon grid, the SAM is not present, and we observe only in the corner a deformed SAM. This behavior differes from the coaxial nanorods bearing crystalline SAM[35] and may point to a soft SAM shell due to weak molecular interaction enabiling reorganization in the presence of neighboring surfaces.

Optical Properties and Morphological of Coaxial Nanorod Thin Films. Thin films were produced on glass substrates by spin coating **1**−**ZnO** from a highly concentrated chlorobenzene solution (∼30 mg/mL). Figure 3b compares the absorption spectra of **1**−**ZnO** in solution and **1**−**ZnO** thin film. Both absorption spectra are similar, but additional light absorption between 600 and 750 nm can be observed in the case of thin films. Such

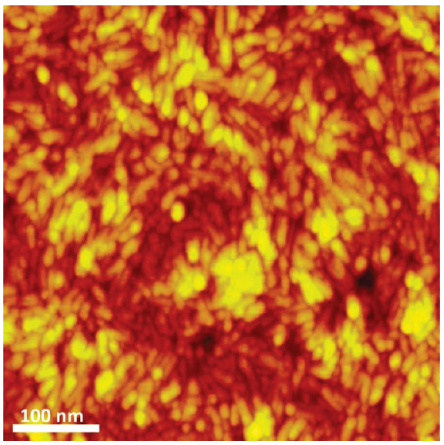

Figure 5. Atomic force microscope analysis of a **1**−**ZnO** film surface performed in tapping mode.

absorption band enlargement may arise from increased $\pi-\pi$ interaction among **1** molecules within the film. The morphology of spin coated **1**−**ZnO** films is probed by HR-TEM as shown in panels c and d of Figure 4. A densely packed layer of hybrid nanorods can be observed. The darker areas represent ZnO nanorods, while the lighter areas correspond to the grafted molecules. The distances between the ZnO nanorods within the film do not exceed a few nanometers over an area of several micrometers indicating a lack of any phase separation between the organic donor and the inorganic acceptor. This is a direct consequence of the direct grafting of the organic p-type semiconductor phase onto the ZnO nanorods. Thus solution processing of the hybrid heterojunctions into thin films leads to nanostructured semiconductor materials with well-controlled D/A phase separation less than the exciton diffusion length of 10 nm. Furthermore atomic force microscope (AFM) analysis is performed to study nanorod aggregation and film surface roughness. We find that the coaxial nanorods form densely packed layers of small parallel oriented aggregates (Figure 5). The average surface roughness is around 5 nm.

As mentioned previously, ZnO nanorods are used to introduce vectorial charge transport along the *c* axis of the nanorod within the film. The optimal orientation of the coaxial nanorods within the film is perpendicular to the electrodes. Angle-resolved X-ray diffraction in in-plane (IP-XRD) and out-of-plane (OOP-XRD) configuration was used to study the average orientation of the nanorods. In general, the XRD pattern of pure ZnO NRs shows three peaks (31.9°, 34.4°, and 36.3°) corresponding to (100), (002), and (111) crystal planes, respectively.[43] The (002) peak, which corresponds to the orientation along the *c* axis, is very sensitive to the orientation of the nanorods. IP-XRD and OOP-XRD graphs of pure ZnO nanorods are shown in Figure S2 (Supporting Information). The (002) peak intensity is much stronger in the IP configuration as compared to OOP. This indicates that pure ZnO nanorods are preferentially oriented parallel to the surface of the substrate. In the case of **1**−**ZnO** nanorods the situation has changed. Both IP and OOP configurations have identical (002) peak intensities (Figure 6) revealing that the orientation of hybrid nanorods within the films is random relative to the substrate. Although such orientation does not represent the ideal case, it can lead to an improvement in charge transport toward the electrodes as compared to isotropic hybrid nanostructures such as nanospheres. The XRD graphs

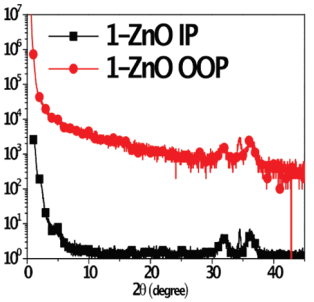

Figure 6. Out-of-plane (OOP) and in-plane XRD analysis of **1**−**ZnO** thin films using 23 wt % of **1**.

give also information about the organization of grafted **1** at the ZnO surface.[35] The absence of any diffraction peaks related to the organic layer in OOP and IP configuration in Figure 6 reveals that molecule **1** forms amorphous layers. This result was found to be independent of the mass ratio and supports our interpretation that the weak hypsochromic shift observed in the absorption spectrum of the grafted compound is related to the lack of crystalline organization among the grafted molecules.

Photovoltaic properties of coaxial nanorod thin films. Usually BHJ solar cells are obtained by mixing donor and acceptor materials at a specific mass ratio. Here, the mixing of the two materials leads directly to nanometer-scale bulk heterojunctions, the coaxial nanorods. In order to form a bicontinuous network of donor and acceptor phases, these coaxial nanorods have to form direct contact between ZnO nanorods as well as a continuous phase of intercalated monolayers. If we consider that ZnO nanorods are covered by a densely packed monolayer of grafted molecules, direct contact between the ZnO nanorods might be difficult. However, if the packing density is lower, which is the case of submonolayers, direct contact between bare ZnO areas or areas of low molecule density should be possible. Submonolayers of different packing density can be obtained by varying the number of grafted molecules per nanorod, i.e., the weight percentage (wt %) of **1** in **1**−**ZnO** nanorods, during synthesis.[35] Here we chose weight percentages between 14 and 28 wt % of **1** which corresponds to an average packing density of 1.4−3.3 molecules/nm^2 ZnO surface. For this calculation, we assume that all molecules are grafted to the surface. The solar cells were prepared via spin coating **1**−**ZnO** from chlorobenzene solution on indium tin oxide (ITO) covered glass substrates, that were coated with poly(3,4-ethylene-dioxythiophene)−poly(styrenesulfonate) (PEDOT−PSS) before. The devices were completed by thermal evaporation of an 80 nm thick aluminum electrode (0.2 cm^2 area). All solar cells were characterized in an inert argon atmosphere (<0.1 ppm H_2O, < 0.1 ppm O_2) using a class AAA solar simulator. Figure 7a illustrates a scheme of the corresponding device structure, while a cross section of a hybrid solar cell obtained by scanning electron microscopy (SEM) is shown in Figure 7b. From this analysis, the thickness of the hybrid layer is determined to approximately 150 nm. Figure 7c gives the current−voltage ($I-V$) curve of a **1**−**ZnO** solar cell using coaxial nanorods obtained from 23 wt % of **1**. The device shows an open circuit voltage of V_{oc} = 0.52 V, a short-circuit current density J_{sc} = 1.63 mA/cm^2, and a fill factor FF = 37% resulting in solar energy conversion efficiency of 0.32%. The external quantum efficiency (EQE) and the internal quantum efficiency (IQE) spectra of the coaxial device using 23 wt % of **1** are shown in Figure 7d. The photocurrent generation matches the absorption

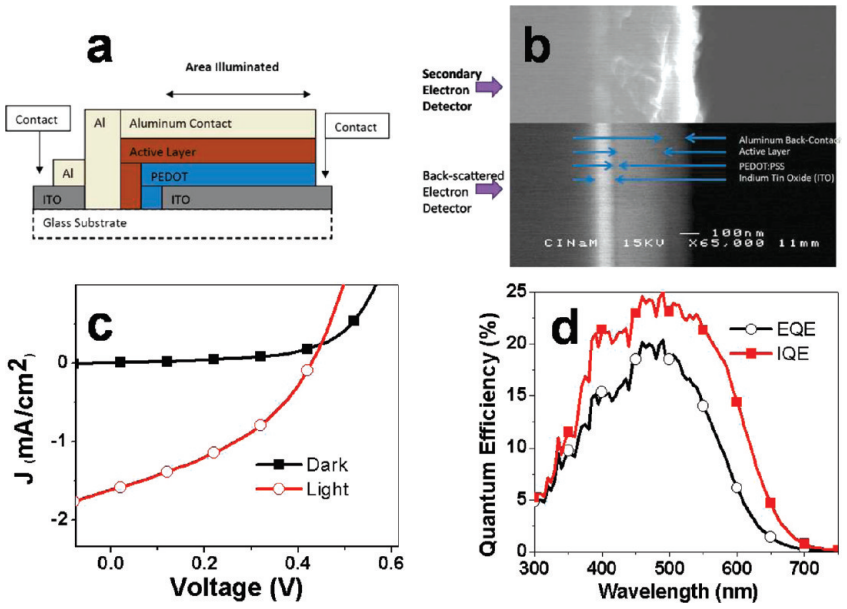

Figure 7. (a) Device structure and (b) corresponding cross section obtained from SEM analysis of the **1**−**ZnO** solar cells. (c) $I-V$ curves in dark and under simulated AM1.5 illumination as well as (d) external and internal quantum efficiencies of typical **1**−**ZnO** devices using 23 wt % of **1**.

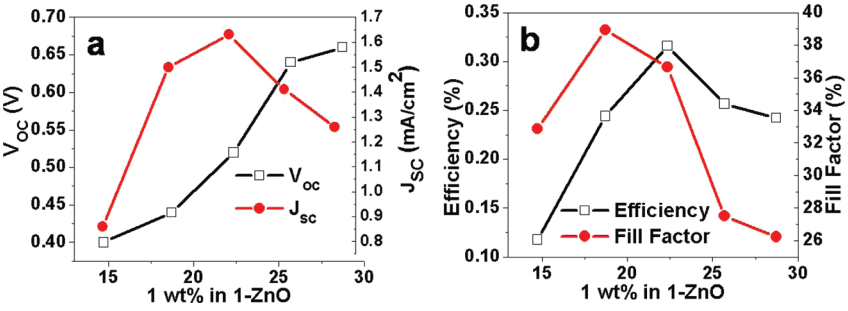

Figure 8. Photovoltaic parameters of **1**−**ZnO** solar cells as a function of wt % of **1**: (a) V_{OC} and J_{SC}, (b) efficiency η and fill factor FF.

spectra of the coaxial nanorod film and the EQE spectrum reaches 20% at the absorption maximum wavelength, while the IQE spectrum of the same device shows 25% at the absorption maximum. The low IQE value might be related to poor charge carrier transport and/or fast charge carrier recombination within the hybrid network. Figure 8 shows how the photovoltaic characteristics of the devices depend on the **1** mass ratio, i.e., packing density of the grafted molecules at the ZnO surface. The open circuit voltage V_{oc} increases with increasing mass ratio as can be seen in Figure 8a. This might be related to a continuous reduction of shunt pathways, which are generated by conducting pathways of ZnO nanorods from one anode to cathode. J_{sc} increases initially when the mass ratio of compound **1** is increased, followed by a decrease for higher mass ratio. The maximum of J_{sc} can be explained by the following consideration. Raising the amount of grafted molecules increases light absorption in the active layer and thus photocurrent generation at the hybrid interface. Furthermore the increase in mass ratio might initially improve the percolation pathways among grafted donor domains. At higher mass ratio, percolation pathways between ZnO nanorods start to be interrupted which leads to a reduction of collected photocurrent. The dependence of the fill factor FF on the mass ratio is rationalized in Figure 8b. The maximum value of FF = 39% at an intermediate mass ratio can be understood by taking into consideration the balance between electron and hole transport. While at low mass ratio hole-only transport might be limited due to weak concentration of donor phases, high mass ratio may probably reduce the contacts between ZnO nanorods and lead to low electron mobility. Therefore we can suppose that both low and high mass ratios lead to unbalanced charge transport and to high internal resistance, which is reflected in the behavior of the FF. Taking into account that ZnO nanorod based hybrid BHJ solar cells have been demonstrated with fill factor up to 62%,[17] it is clear that the charge carrier transport within the hybrid coaxial network is still limited, even for an optimized mass ratio. Possible reasons are poor percolation within the ZnO network due to the presence of a high amount of surfactants and/or low hole mobility in the organic phase. Further studies are necessary to answer this question and will be addressed in the future work. Combining the trends of all parameters, we obtain an optimal mass ratio of 23 wt % with a solar energy conversion efficiency of 0.32%, which corresponds to 2.3 molecules/nm^2 before film formation.

A simple model of hybrid coaxial nanorod solar cells can be proposed from the analysis above. The conducting contact between ZnO nanorods may occur at bare ZnO surfaces, which

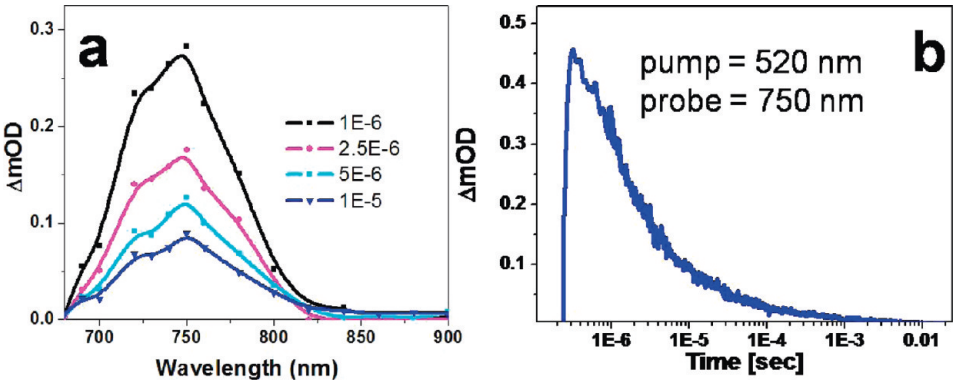

Figure 9. (a) Transient absorption spectra at different times after excitation and (b) transient absorption decay of a **1**−**ZnO** film using 23 wt % of **1**.

are free or almost free of molecules. This can be obtained by using partly covered nanorods. Alternatively it is possible that molecule migration during film formation may allow to lay open bare ZnO areas locally. Indeed molecular reorganization after grafting has been observed in our earlier study.[35] Furthermore the presented HR-TEM analyses give some indications that the SAM morphology may be different after film formation leading to short distances between ZnO nanorods locally.

In order to answer question whether the device performance is limited by light absorption, we estimate the volume percentage of the organic phase inside the hybrid thin film by using a molecule packing density of 4 molecules/nm^2, which was measured for crystalline SAM on coaxial nanorods,[36] as upper limit. For 23 wt % of compound **1** in **1**−**ZnO**, which corresponds to the optimal mass ratio, a volume percentage of the organic phase around 40 vol % is found. This value corresponds to a typical polymer content in polymer−nanoparticle blends.[7−26] Thus the donor phase in these hybrid films has comparable light absorption properties although it is constituted only by grafted submonolayers and represents not a limitation for high solar cell performances.

Time-Resolved Transient Absorption Spectroscopy. The photoinduced electron-transfer yield and charge recombination of the coaxial nanorod BHJ were further studied using micro- to millisecond time-resolved transient absorption spectroscopy (TAS) on **1**−**ZnO** thin films of a 23 wt % of **1** deposited on ITO. Due to the fact that the donor phase is only composed of grafted monolayers and large donor−acceptor interfaces are present in the hybrid films, fast charge carrier recombination could be a limiting factor for these solar cells. Figure 9a shows the transient absorption spectra of **1**−**ZnO** thin films at different times after excitation at 520 nm. A wide absorption band, assigned to the radical cation band, appears with an absorption maximum at λ_{max} = 750 nm. Charge carrier recombination is then studied using excitation and probe wavelengths of 520 and 750 nm, respectively. The TAS decay analysis of a **1**−**ZnO** thin film is shown in the Figure 9b. Importantly the recombination half-time of the radical cation band is 6 μs which is relatively long-lived and comparable to typical blends of poly(3-hexylthiophene) (P3HT) and phenyl-C61-butyric acid methyl ester (PCBM).[44,45] The relatively slow recombination rate is surprising if one takes into account the high D/A interfacial area and the monolayer thick donor phase. One possible explanation for this might be that electrons and holes are not localized on the same coaxial nanostructures after photoexcitation but distributed over several monolayer phases and ZnO NRs, respectively.

CONCLUSIONS

We have demonstrated a novel architecture for hybrid bulk heterojunctions solar cells. Hybrid coaxial heterojunction nanostructures based on surface functionalized ZnO nanorods allow simple processing of bulk heterojunction layers consisting of controlled donor domain sizes smaller than typical exciton diffusion length. Transient absorption spectroscopy analysis reveals that charge carrier recombination kinetics of the coaxial nanorod films are comparable to highly efficient polymer/fullerene blends, which allows efficient charge carrier extraction. The corresponding solar cells reveal that the device performance is controlled by the mass ratio between the grafted molecules and the ZnO nanorods similar to classical polymer blends. Our future work will focus on a deeper understanding of charge transport within the organic and inorganic phase of the interpenetrating network, which is necessary to further increase power conversion efficiencies of the devices.

ASSOCIATED CONTENT

Supporting Information. Synthesis of molecule **1** and figures showing cyclic voltammogram of **1** and XRD analysis of ZnO nanorod thin films. This material is available free of charge via the Internet at http://pubs.acs.org.

AUTHOR INFORMATION

Corresponding Author

*E-mail: ackermann@cinam.univ-mrs.fr, fages@cinam.univ-mrs.fr.

ACKNOWLEDGMENT

The authors acknowledge financial support from OSEO and VALORPACA (Grant NANOHYBA), P.A. acknowledges the Spanish Ministry of Science and Innovation for a postdoc grant, and T.I. and J.N. acknowledge EPSRC for research Grants EP/G031088/1 and EP/E036341

REFERENCES

(1) Yu, G.; Gao, J.; Hummelen, J. C.; Wudl, F.; Heeger, A. J. *Science* **1995**, *270*, 1789.
(2) Yang, F.; Shtein, M.; Forrest, S. R. *Nat. Mater.* **2005**, *4*, 37.
(3) Shaheen, S. E.; Radspinner, R.; Peyghambarian, N. *Appl. Phys. Lett.* **2001**, *79*, 2996.
(4) Brabec, C. J.; Gowrisanker, S.; Halls, J. J. M.; Laird, D.; Jia, S.; Williams, S. P. *Adv. Mater.* **2010**, *22*, 3839.

(5) http://www.pv-tech.org/ (last accessed November 2010).
(6) Bouclé, J; Ravirajan, P; Nelson, J *J. Mater. Chem.* **2007**, *17*, 3141.
(7) W. Huynh, W. U.; Dittmer, J.; Alivisatos, A. P. *Science* **2002**, *295*, 2425.
(8) Sun, B.; Snaith, H. J.; Dhoot, A. S.; Westenhoff, S.; Greenham, N. C. *J. Appl. Phys.* **2005**, *97*, 014914.
(9) Coakley, K. M.; McGehee, M. D. *Appl. Phys. Lett.* **2003**, *83*, 3380.
(10) Chang, C. H.; Huang, T. K.; Lin, Y. T.; Lin, Y. Y.; Chen, C. W.; Chu, T. H.; Su, W. F. *J. Mater. Chem.* **2008**, *18*, 2201.
(11) Ravirajan, P.; Haque, S. A.; Durrant, J. R.; Bradley, D. D. C.; Nelson, J. *Adv. Funct. Mater.* **2005**, *15*, 609.
(12) Kwong, C. Y.; Choy, W. C.; Djurisic, A. B.; Chui, P. C.; Cheng, K. W.; Chan, W. K. *Nanotechnology* **2004**, *15*, 1156.
(13) Cherian, S.; Wamser, C. C. *J.Phys. Chem. B* **2000**, *104*, 3624.
(14) Bouclé, J.; Chyla, S.; Shaffer, M. S. P.; Durrant, J. D.; Bradley, D. C. D.; Nelson, J. *Adv. Funct. Mater.* **2008**, *18*, 622.
(15) Lin, Y. Y.; Chu, T. H.; Li, S. S.; Chuang, C. H.; Chang, C. H.; Su, W. F.; Chang, C. P.; Chu, M. W.; Chen, C. W. *J. Am. Chem. Soc.* **2009**, *131*, 3644.
(16) Ravirajan, P.; Peiro, A. M.; Nazeeruddin, M. K.; Graetzel, M.; Bradley, D. C. D.; Durrant, J. R.; Nelson, J. *J. Phys. Chem. B* **2006**, *110*, 7635.
(17) Beek, W. J. E.; Wienk, M. M.; Kemerink, M.; Yang, X.; Janssen, R. A. J. *J. Phys. Chem. B* **2005**, *109*, 9505.
(18) Oosterhout, S. D.; Wienk, M. M.; Van Bavel, S. S.; Thiedmann, R.; Koster, L. J. A.; Gilot, J.; Loos, J.; Schmidt, V.; Janssen, R. A.J. *Nat. Mater.* **2009**, *8*, 818.
(19) Shao, S.; Liu, F.; Xie, Z.; Wang, L. *J. Phys. Chem. C.* **2010**, *114*, 9161.
(20) Said, A. J.; Poize, G.; Martini, C.; Ferry, D.; Marine, W.; Giorgio, S.; Fages, F.; Hocq, J.; Bouclé, J.; Nelson, J.; Durrant, J. R.; Ackermann, J. *J. Phys. Chem. C* **2010**, *114* (25), 11273–11278.
(21) Krebs, F. C. *Sol. Energy Mater. Sol. Cells* **2008**, *92*, 715–726.
(22) Sharma, G. D.; Suresh, P.; Balaraju, P.; Sharma, S. K.; Roy, M. S. *Synth. Met.* **2008**, *158*, 400.
(23) McDonald, S. A.; Konstantatos, G.; Zhang, S.; Cyr, P. W.; Klem, E. J. D.; Levina, L.; Sargent, E. H. *Nat. Mater.* **2005**, *4*, 138.
(24) Noone, K. M.; Strein, E.; Anderson, N C.; Wu, P.; Jenekhe, S. A.; Ginger, D. S. *Nano Lett.* **2010**, *10*, 2635.
(25) Liu, C. Y.; Holman, Z. C.; Kortshagen, U. R. *Nano Lett.* **2009**, *9*, 449.
(26) Liu, C. Y.; Holman, Z. C.; Kortshagen, U. R. *Adv. Funct. Mater.* **2010**, *20*, 1–8.
(27) Gur, I.; Fromer, N. A.; Chen, C.-P.; Kanaras, A. G.; Alivisatos, A. P. *Nano Lett.* **2007**, *7*, 409–414.
(28) Palaniappan, K.; Murphy, J. W.; Khanam, N.; Horvath, J.; Alshareef, H.; Quevedo-Lopez, M.; Biewer, M. C.; Park, S. Y.; Kim, M. J.; Gnade, B. E.; Stefan, M. C. *Macromolecules* **2009**, *42* (12), 3845–3848.
(29) Gur, I.; Former, N. A.; Alivisatos, A. P. *J. Phys. Chem. B* **2006**, *110*, 25543–25546.
(30) Sun, B.; Snaith, H. J.; Dhoot, A. S.; Westenhoff, S.; Greenham, N. C. *J. Appl. Phys.* **2005**, *97*, 014914.
(31) Snaith, H. J.; Whiting, G. L.; Sun, B.; Greeham, N. C.; Huck, W. T. S.; Friend, R. H. *Nano Lett.* **2005**, *5*, 1653–1657.
(32) Greenham, N. C.; Peng, X.; Alivisatos, A. P. *Phys. Rev. B* **1996**, *54*, 17628.
(33) Liu, J.; Tanaka, T.; Sivula, K.; Alivisatos, A. P.; Fréchet, J. M.J. *J. Am. Chem. Soc.* **2004**, *126*, 6550.
(34) Videlot-Ackermann, C.; Ackermann, J.; Brisset, H.; Kawamura, K.; Yoshimoto, N.; Raynal, P.; El-Kassmi, A.; Fages, F. *J. Am. Chem. Soc.* **2005**, *127*, 16346.
(35) Martini, C.; Poize, G.; Ferry, D.; Kanehira, D.; Yoshimoto, N.; Ackermann, J.; Fages, F. *ChemPhysChem* **2009**, *10*, 2465.
(36) Briseno, A. L.; Holcombe, T. W.; Boukai, A. I.; Garnett, E. C.; Shelton, S. W.; Frechet, J. J. M.; Yang, P. *Nano Lett.* **2010**, *10*, 334.
(37) Cravino, A.; Leriche, P.; Alévêque, O.; Roquet, S.; Roncali, J. *Adv. Mater.* **2006**, *18*, 3033.
(38) Roquet, S.; Cravino, A.; Leriche, P.; Alévêque, O.; Frère, P.; Roncali, J. *J. Am. Chem. Soc.* **2006**, *128*, 3459.
(39) Kageyama, H.; Ohishi, H.; Tanaka, M.; Ohmori, Y. *Adv. Funct. Mater.* **2009**, *19*, 1.
(40) Miura, A.; Chen, Z.; Uji-I, H.; De Feyter, S.; Zdanowska, M; Jonkheijm, P.; Schenning, A. P. H. J.; Meijer, E. W.; Würthner, F.; De Schryver, F. C. *J. Am. Chem. Soc.* **2003**, *125*, 14968.
(41) Didane, Y.; Marsal, P.; Fages, F.; Kumagai, A.; Yoshimoto, N.; Brisset, H.; Videlot-Ackermann, C. *Thin Solid Films* **2010**, *519*, 578.
(42) Hagfeldt, A.; Graetzel, M/ *Chem. Rev.* **1995**, *95*, 49.
(43) Ong, B. S.; Li, C.; Li, Y.; Wu, Y.; Loutfy, R. *J. Am. Chem. Soc.* **2007**, *129*, 2750.
(44) Clarke, T. M.; Jamieson, F. C.; Durrant, J. R. *J. Phys. Chem. C* **2009**, *113*, 20934.
(45) Kim, Y.; Cook, S.; Tuladhar, S. M.; Choulis, S. A.; Nelson, J.; Durrant, J. R.; Bradley, D. D. C.; Giles, M.; Mcculloch, I.; Ha, C. S.; Ree, M. *Nat. Mater.* **2005**, *5*, 197.